Available online at www.sciencedirect.com
SCIENCE DIRECT®
Journal of Computational Physics 195 (2004) 143–152
JOURNAL OF COMPUTATIONAL PHYSICS
www.elsevier.com/locate/jcp

Multistage explicit advective prediction for projection-type incompressible flow solvers

Rainald Löhner *

School of Computational Science and Informatics, M.S. 4C7, George Mason University, 4400 University Drive, Fairfax, VA 22030-4444, USA

Received 10 January 2003; received in revised form 30 July 2003; accepted 29 September 2003

Abstract

A multistep advective predictor has been developed within the context of projection schemes for incompressible flows. The key idea is to integrate with schemes of different order the different regions of the domain. In regions where advection dominates, multistepping yields a considerable benefit. In those regions where viscosity dominates, the scheme reverts naturally to the original one-step scheme. Several examples show savings of the order of 1:3–1:10 as compared with standard projection schemes, even for transient problems. Given that these benefits can be achieved with a very modest change in existing codes, the proposed multistage advective predictor should be widely applicable.

Keywords: Incompressible flow solvers; Projection schemes; Multistage Runge–Kutta; FEM; CFD

1. Introduction

Among the flows that are of importance and interest, the category of low Mach-number or incompressible flows is by far the largest. Most of the products we use on a daily basis have been incompressible flows during their manufacture (polymer extrusion, melts, a large number of food products, etc.). The air which surrounds us can be considered, in almost all instances, as an incompressible fluid (airplanes flying at low Mach-numbers, flows in and around cars, vans, buses, trains and buildings). The same applies to water (ships, submarines, torpedoes, pipes, etc.) and most biomedical liquids (e.g., blood). Given this large number of possible applications, it is not surprising that numerical methods to simulate incompressible flows have been developed for many years, as evidenced by an abundance of the literature [5,7,21].

In order to fix the notation, the equations describing incompressible, Newtonian flows are written as

$$\mathbf{v},t + \mathbf{v}\nabla\mathbf{v} + \nabla p = \nabla\mu\nabla\mathbf{v}, \tag{1}$$

* Tel.: +1-703-993-4075; fax: +1-703-993-4064.
E-mail address: rlohner@gmu.edu (R. Löhner)

0021-9991/$ - see front matter
doi:10.1016/j.jcp.2003.09.025

$$\nabla \cdot \mathbf{v} = 0. \tag{2}$$

Here p denotes the pressure, $\mathbf{v}$ the velocity vector and both the pressure p and the viscosity μ have been normalized by the (constant) density ρ. For most of the applications listed above, the important physical phenomena propagate with the *advective* timescales. We will therefore assume that the advective terms require an explicit time integration. Diffusive phenomena typically occur at a much faster rate, and can/should therefore be integrated implicitly. Given that the pressure establishes itself immediately through the pressure-Poisson equation, an implicit integration of pressure is also required. The hyperbolic character of the advection operator and the elliptic character of the pressure-Poisson equation have led to a number of so-called projection schemes. The key idea is to predict first a velocity field from the current flow variables without taking the divergence constraint into account. In a second step, the divergence constraint is enforced by solving a pressure-Poisson equation. The velocity increment can therefore be separated into an advective–diffusive and pressure increment

$$\mathbf{v}^{n+1} = \mathbf{v}^n + \Delta\mathbf{v}^{\mathrm{a}} + \Delta\mathbf{v}^{\mathrm{p}} = \mathbf{v}^* + \Delta\mathbf{v}^{\mathrm{p}}. \tag{3}$$

For an explicit (forward Euler) integration of the advective terms, with implicit integration of the viscous terms, one complete timestep is given by:

Advective–diffusive prediction: $\mathbf{v}^n \rightarrow \mathbf{v}^*$

$$\left[\frac{1}{\Delta t} - \theta\nabla\mu\nabla\right](\mathbf{v}^* - \mathbf{v}^n) + \mathbf{v}^n \cdot \nabla\mathbf{v}^n + \nabla p^n = \nabla\mu\nabla\mathbf{v}^n. \tag{4}$$

Pressure correction: $p^n \rightarrow p^{n+1}$

$$\nabla \cdot \mathbf{v}^{n+1} = 0, \tag{5}$$

$$\frac{\mathbf{v}^{n+1} - \mathbf{v}^*}{\Delta t} + \nabla(p^{n+1} - p^n) = 0, \tag{6}$$

which results in

$$\nabla^2(p^{n+1} - p^n) = \frac{\nabla \cdot \mathbf{v}^*}{\Delta t}. \tag{7}$$

Velocity correction: $\mathbf{v}^* \rightarrow \mathbf{v}^{n+1}$

$$\mathbf{v}^{n+1} = \mathbf{v}^* - \Delta t\nabla(p^{n+1} - p^n). \tag{8}$$

At steady state, $\mathbf{v}^* = \mathbf{v}^n = \mathbf{v}^{n+1}$ and the residuals of the pressure correction vanish, implying that the result does not depend on the timestep Δt. θ denotes the implicitness-factor for the viscous terms ($\theta = 1$: first order, fully implicit, $\theta = 0.5$: second order, Crank–Nicholson). The forward Euler integration of the advection terms imposes rather severe restrictions on the allowable timestep. For this reason, alternative explicit integration schemes have been used repeatedly [22]. Many authors have used multilevel schemes, such as the second-order Adams–Bashforth scheme. The problem with schemes of this kind is that they use the values at the current and previous timestep, which makes them awkward in the context of adaptive refinement, moving meshes, and local or global remeshing. For this reason, single step schemes are preferable. Lax–Wendroff or Taylor–Galerkin schemes offer such a possibility, but in this case the result of steady-state calculations depends (albeit weakly) on the timestep (or equivalently the Courant-number) chosen. For this reason, single step schemes whose steady-state result does not depend on the timestep are preferable. Projection schemes of this kind (explicit advection with a variety of schemes, implicit diffusion,

pressure-Poisson equation for either the pressure or pressure increments) have been widely used in conjunction with spatial discretizations based on finite differences [1–3,13], finite volumes [10], and finite elements [4,6,11,12,14–18,20].

2. Multistep discretization of advective terms

The scheme given by Eqs. (4)–(8) is, at best, of second order in time. It is surprising to note that apparently no attempt has been made to use multistage explicit schemes to integrate the advective terms with higher order or to accelerate the convergence to steady state. This may stem from the fact that the implicit integration of the viscous terms apparently impedes taking the full advantage multistage schemes offer for the Euler limit of no viscosity. An interesting alternative, proposed here, is to integrate with different timestepping schemes the different regimes of flows with highly variable cell Reynolds-number

$$Re_h = \frac{\rho|\mathbf{v}|h}{\mu}, \tag{9}$$

where h is the mesh size. For the case $Re_h < 1$ (viscous dominated), the accuracy in time of the advective terms is not so important. However, for $Re_h > 1$ (advection dominated), the advantages of higher order time-marching schemes for the advective terms are considerable, particularly if one considers vortex transport over large distances. Dahlquist's theorem states that no unconditionally stable, implicit one-step scheme can be of order higher than two (this being the Crank–Nicholson scheme). However, explicit schemes of the Runge–Kutta type can easily yield higher order timestepping. A k-step, time-accurate Runge–Kutta scheme or order k for the advective parts may be written as

$$\mathbf{v}^i = \mathbf{v}^n + \alpha^i \gamma \Delta t\left(- \mathbf{v}^{i-1} \cdot \nabla \mathbf{v}^{i-1} - \nabla p^n + \nabla \mu \nabla \mathbf{v}^{i-1}\right); \quad i = 1,\ k-1, \tag{10}$$

$$\left[\frac{1}{\Delta t} - \theta \nabla \mu \nabla\right]\left(\mathbf{v}^k - \mathbf{v}^n\right) + \mathbf{v}^{k-1} \cdot \nabla \mathbf{v}^{k-1} + \nabla p^n = \nabla \mu \nabla \mathbf{v}^{k-1}. \tag{11}$$

Here, the α^i are the standard Runge–Kutta coefficients $\alpha^i = 1/(k+1-i)$. As compared to the original scheme given by Eq. (4), the $k-1$ stages of Eq. (10) may be seen as a predictor (or replacement) of $\mathbf{v}^n$ by $\mathbf{v}^{k-1}$. The original right-hand side has not been modified, so that at steady-state $\mathbf{v}^n = \mathbf{v}^{k-1}$, preserving the requirement that the steady-state be independent of the timestep Δt. The factor γ denotes the local ratio of the stability limit for explicit timestepping for the viscous terms versus the timestep chosen. Given that the advective and viscous timestep limits are proportional to

$$\Delta t_{\mathrm{a}} \approx \frac{h}{|\mathbf{v}|}; \quad \Delta t_{\mathrm{v}} \approx \frac{\rho h^2}{\mu}, \tag{12}$$

we immediately obtain

$$\gamma = \frac{\Delta t_{\mathrm{v}}}{\Delta t_{\mathrm{a}}} \approx \frac{\rho|\mathbf{v}|h}{\mu} \approx Re_h, \tag{13}$$

or, in its final form

$$\gamma = \min(1, Re_h). \tag{14}$$

In regions away from boundary layers, this factor is O(1), implying that a high-order Runge–Kutta scheme is recovered. Conversely, for regions where $Re_h = \mathrm{O}(0)$, the scheme reverts back to the original one (Eq.

(4)). Note also that the very tempting option of ignoring the pressure and viscous terms in Eq. (10) leads to steady-state results are not independent of the timestep.

Besides higher accuracy, an important benefit of explicit multistage advection schemes is the larger timestep one can employ. The increase in allowable timestep is roughly proportional to the number of stages used (and has been exploited extensively for compressible flow simulations [9]). Given that for an incompressible solver of the projection type given by Eqs. (4)–(9) most of the CPU time is spent solving the pressure-Poisson system Eq. (5), the speedup achieved is also roughly proportional to the number of stages used.

3. Examples

The multistage advection scheme described above was implemented in FEFLO, an edge-based finite element solver using linear elements [16], and was tested on a variety of examples, a few of which are included here. We remark from the outset that the main aim of the comparison is the relative speed of the different schemes. Given that the discretization of fluxes is the same for one-stage and multistage explicit advection, no change in results occurs for steady flow cases. The changes for time-accurate calculations are shown for the respective cases. Detailed comparison to experiments, mesh refinement studies, etc. of the basic scheme used in FEFLO may be found in [6,11,12,14,16,20].

For the steady flow cases, local timesteps were used to accelerate convergence. Moreover, the Courant-numbers cited in the comparisons are the largest ones that still yielded stable solutions, and were all based solely on the advective terms (as stated before, the viscous terms are always integrated implicitly).

All runs were performed on a PC with an Intel-P4 processor running at 2.1 GHz with 1 Gbyte of RAM using the Intel Fortran compiler under Red Hat Linux.

3.1. NACA0012

The first example considered is the classic NACA0012 wing at $\alpha = 5°$ angle of attack. This is a steady, inviscid case (Euler). Figs. 1(a) and (b) show the surface mesh employed, as well as the surface pressures obtained. The mesh consisted of `nelem=368,872` elements and `npoin=68,321` points.

Each of these runs was considered converged when the change in lift, normalized by the Courant-number, was below $t_l = 10^{-3}$ for five subsequent timesteps. We have found such a measure to be a better indicator of convergence than residuals, as this allows the user to state clearly which degree of accuracy is desired. Figs. 1(c) and (d) show the convergence history for the lift and residuals respectively. One can see that the multistage advection schemes converge significantly faster. The timings obtained have been summarized in Table 1. Here, as in the subsequent tables, the notation Ex-k refers to explicit advection with a k-state Runge–Kutta scheme (Eq. (10)). The timings indicate that this faster convergence also translates into a marked reduction in CPU requirements.

3.2. Wigley Hull

The second example considered is the well-known Wigley Hull, given by the analytical formula

$$y = 0.5 \cdot B \cdot \left[1 - 4x^2\right] \cdot \left[1 - \left(\frac{z}{D}\right)^2\right],$$

where B and D are the beam and the draft of the ship at still water. The case considered here, which had $D = 0.0625$, $B = 0.1$, has been studied before by Löhner et al. [16]. This is a steady, inviscid case (Euler)

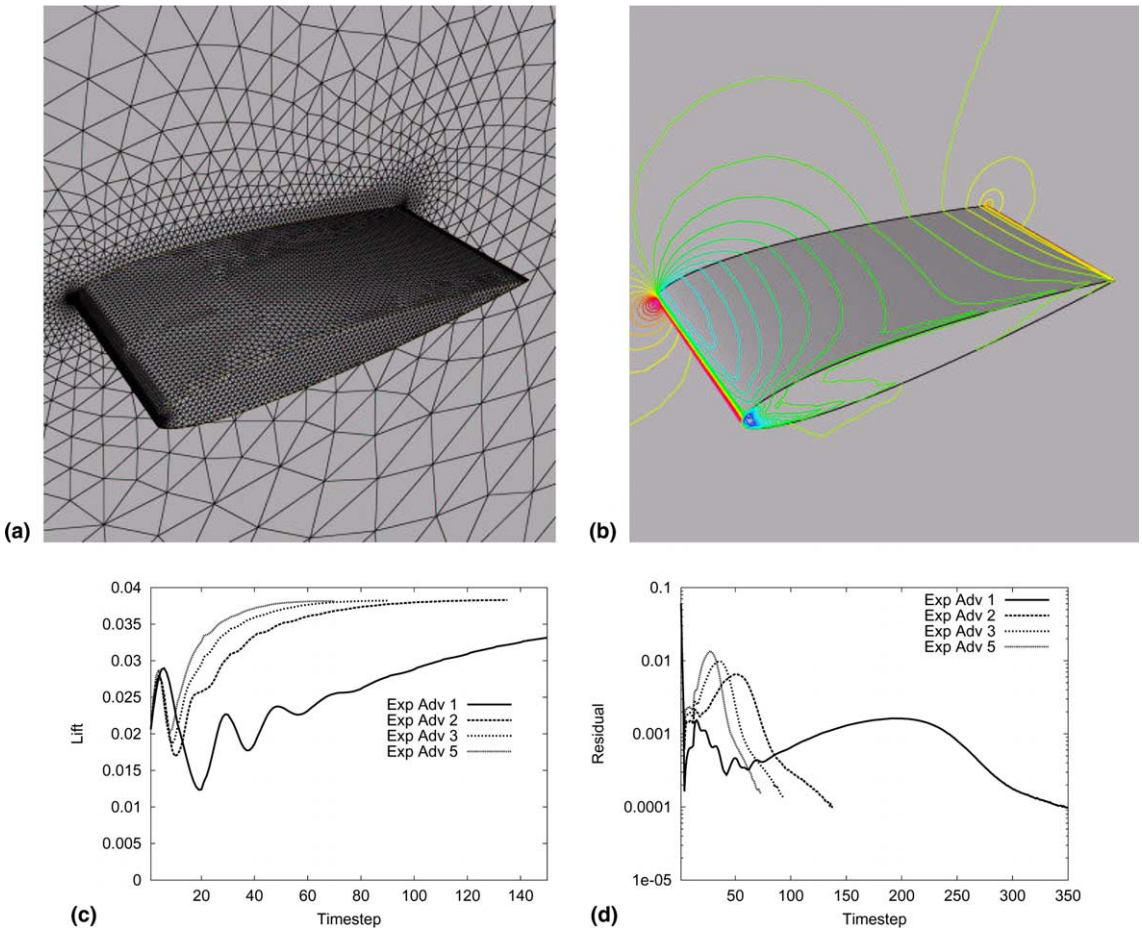

Fig. 1. (a) and (b) NACA 0012: surface mesh and pressure. (c) and (d) NACA 0012: convergence history for lift and residuals.

with free surface (no mesh movement, i.e., geometric free surface conditions). Figs. 2(a) and (b) show the surface mesh employed (the volume mesh had `nelem = 360, 247`, `npoin = 67, 785`), as well as the free surface obtained.

Figs. 2(c) and (d) show the convergence history for the wavedrag and residuals respectively. The wavedrag coefficient obtained for the present mesh was $c_w = 0.532 \times 10^{-4}$, and compares favourably with the experimental data of $c_w = 0.567 \times 10^{-4}$ [8] and the moving mesh result of $c_w = 0.607 \times 10^{-4}$ [16]. One

Table 1
NACA-0012

Scheme	CFL	`ntime`	CPU (s)	Speedup
Ex 1	0.1	540	579	1.00
Ex 2	0.4	135	193	3.00
Ex 3	0.6	90	157	3.69
Ex 5	0.8	70	166	3.48

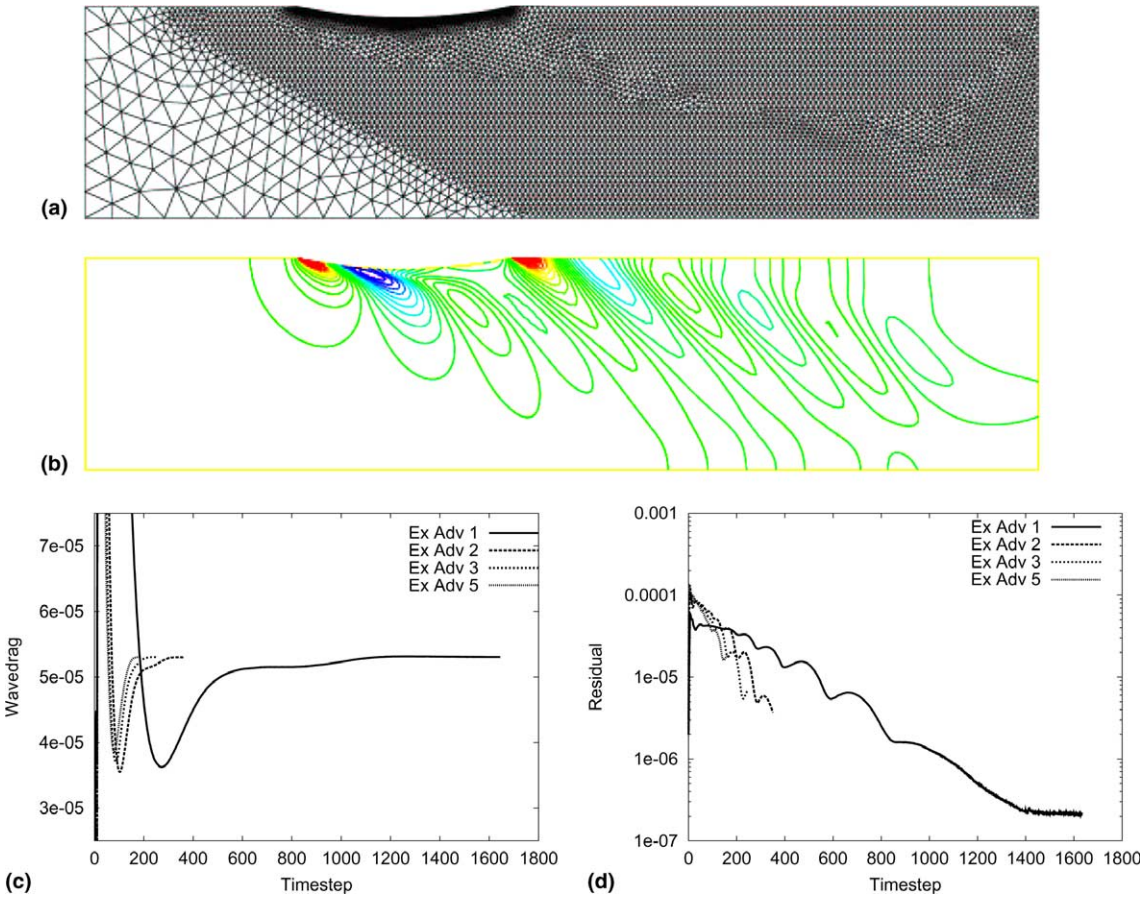

Fig. 2. (a) and (b) Wigley Hull: surface mesh and free surface elevation. (c) and (d) Wigley Hull: convergence history for lift and residuals.

Table 2
Wigley Hull

Scheme	CFL	ntime	CPU (s)	Speedup
Ex 1	0.1	1910	3232	1.00
Ex 2	0.4	350	890	3.63
Ex 3	0.6	235	778	4.15

Table 3
von Karman vortex street

Scheme	CFL	Δt	ntime	CPU (s)	Speedup
Ex 1	0.1	O(0.002)	9961	12,929	1.00
Ex 2	0.4	O(0.008)	2490	4194	3.08
Ex 3	0.6	O(0.012)	1660	3296	3.92
Ex 5	0.8	O(0.016)	1245	3201	4.03
Ex 5	1.2	O(0.025)	830	1546	8.36
Ex 5	1.6	O(0.033)	623	1114	11.60
Ex 5	1.8	O(0.037)	554	995	12.99

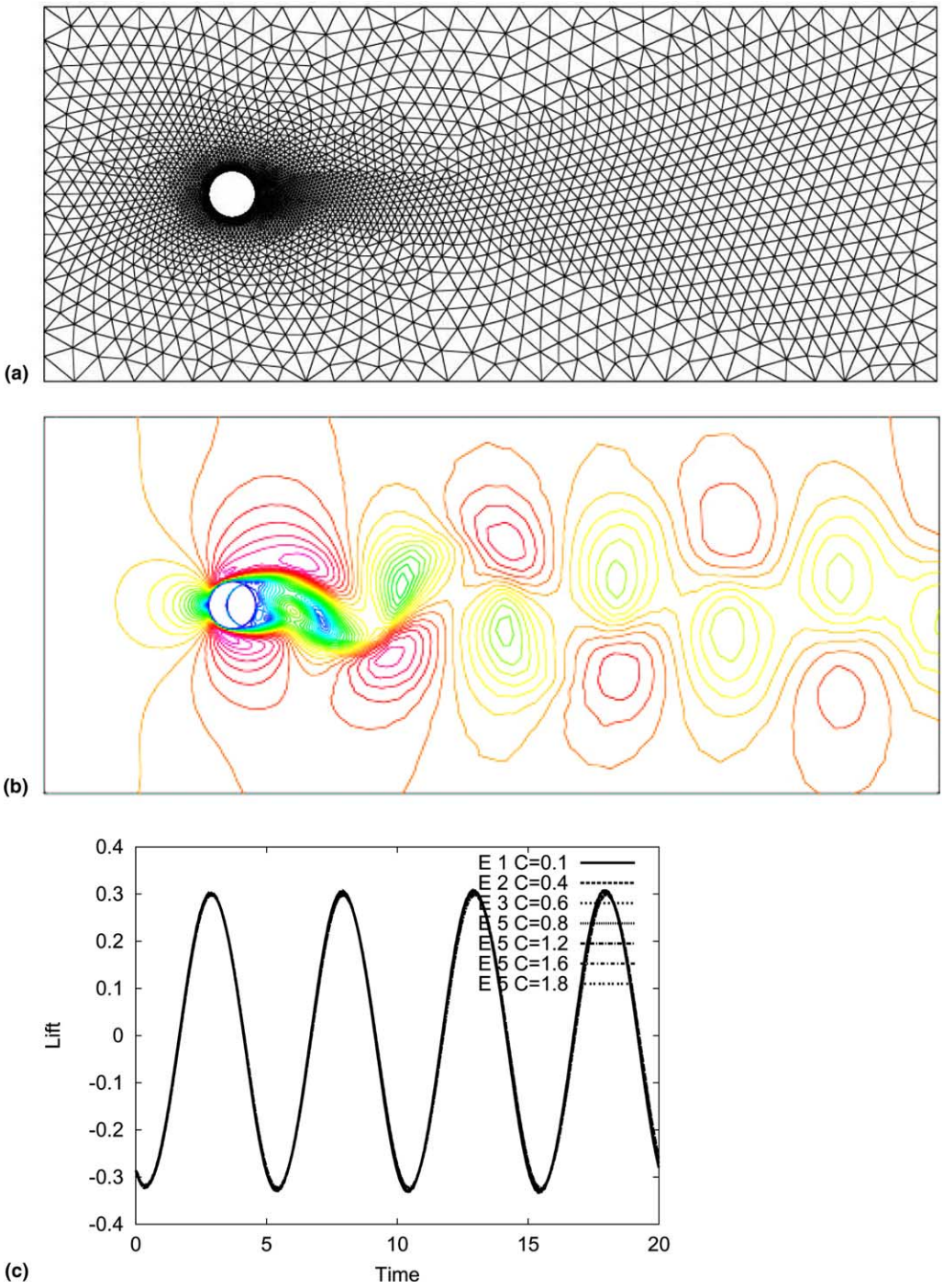

Fig. 3. (a) von Karman vortex street: surface mesh. (b) von Karman vortex street: abs(velocity) in plane. (c) von Karman vortex street: lift history.

can see that, as before, the multistage advection schemes converge significantly faster. The timings, summarized in Table 2, confirm a considerable speedup.

3.3. von Karman Vortex street

The third example considered is also a well-known benchmark case [19]. A circular cylinder is suspended in a uniform stream of incompressible fluid. The separation at the back of the cylinder generates the so-called von Karman vortex street, whose characteristics depend on the Reynolds number

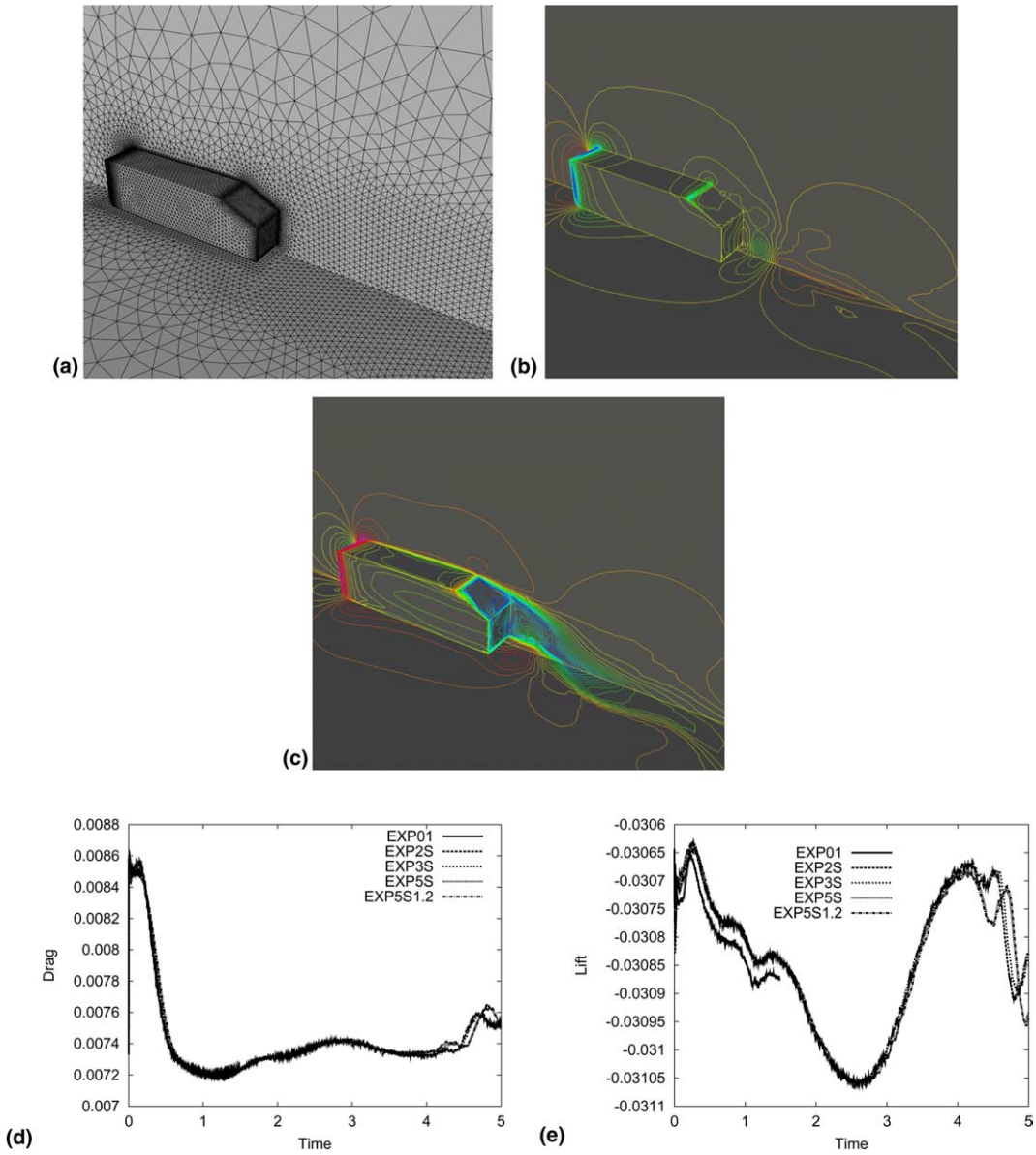

Fig. 4. (a) and (b) Ahmed body: surface mesh and pressure. (c) Ahmed body: surface speed. (d) and (e) Ahmed body: drag and lift history.

Table 4
Ahmed body

Scheme	CFL	Δt	ntime	CPU (s)	Speedup
Ex 1	0.1	O(0.0003)	3362	12,047	1.00
Ex 2	0.4	O(0.0012)	847	3785	3.18
Ex 3	0.6	O(0.0018)	563	3224	3.74
Ex 5	1.0	O(0.0030)	339	2840	4.24
Ex 5	1.2	O(0.0035)	282	2420	4.97

$$Re = \frac{\rho V_\infty D}{\mu},$$

where D denotes the diameter of the cylinder. This is essentially a 2-D example, but was run with the 3-D solver. A mesh of nelem = 113,056, npoin = 23,228 was used for the simulation, with special placement of points in the vicinity of the cylinder. The parameters were chosen such that the resulting Reynolds number was $Re = 190$.

Figs. 3(a) and (b) show the surface grid and the absolute value of the velocity in a cut plane. In order to compare the different schemes, the run was started impulsively using the one-stage explicit-advection scheme. The run was continued until the vortex street was fully developed. Starting from this (restart) state, the different schemes were exercised and compared to one another. The lift of the cylinder as a function of time for the original explicit-advection projection scheme and the multistage advection schemes is displayed in Fig. 3(c), and Table 3 summarize the results.

Observe that for all the explicit-advection multistep schemes, the results are almost identical. The Strouhal number obtained is approximately $S = 0.2$, in good agreement with experiments [19].

3.4. Ahmed car body

The fourth example considered is high Reynolds-number flow past the so-called Ahmed body. This is a standard test case for external car aerodynamics. The parameters were set to: $\rho = 1.0$, $\mathbf{v} = (1, 0, 0)$, $\mu = 2.33 \times 10^{-7}$, $L = 1$, which implies a Reynolds-number of $Re = 4.29 \times 10^6$. The $k - \epsilon$ turbulence model was used. The resulting flow is quasi-steady and shows the development of a vortex train behind the body. Figs. 4(a)–(c) show the surface mesh employed, as well as the pressure and velocity field obtained. Note the boundary layer mesh (the complete mesh consisted of (nelem = 420,245, npoin = 77,279).

This unsteady problem was solved using the different explicit schemes. Figs. 4(d) and (e) show the forces computed, and Table 4 summarizes the runs. Note that the drag and lift curves are not identical for all schemes, but that the differences are small. This is to be expected for the $k - \epsilon$ turbulence model, where small changes can have a pronounced effect as the solution evolves. The speedups are not as high as in the case of the laminar cylinder flow, as a significant amount of CPU time is spent updating the $k - \epsilon$ equations. Nevertheless, speed-ups of the order of O(1:4) are realized.

4. Conclusions

A multistep advective predictor has been developed within the context of projection schemes for incompressible flows. The key idea is to integrate with schemes of different order the different regions of the domain. In those regions where advection dominates, multistepping yields a considerable benefit. In those regions where viscosity dominates, the scheme reverts naturally to the original one-step scheme.

Several examples show savings of the order of 1:3–1:10 as compared with standard projection schemes, even for transient problems. Given that these benefits can be achieved with a very modest change in existing codes, the proposed multistage advective predictor should be widely applicable.

Acknowledgements

This work was partially supported by ONR and AFOSR. The technical monitors were Drs. Patrick Purtell and Leonidas Sakell.

References

[1] B. Alessandrini, G. Delhommeau, A multigrid velocity–pressure–free surface elevation fully coupled solver for calculation of turbulent incompressible flow around a hull, in: Proceeding of the 21st Symposium on Naval Hydrodynamics, Trondheim, Norway, June, 1996.
[2] J.B. Bell, P. Colella, H. Glaz, A second-order projection method for the Navier–Stokes equations, J. Comput. Phys. 85 (1989) 257–283.
[3] J.B. Bell, D.L. Marcus, A second-order projection method for variable-density flows, J. Comput. Phys. 101 (1992) 2.
[4] R. Codina, Pressure stability in fractional step finite element methods for incompressible flows, J. Comput. Phys. 170 (2001) 112–140.
[5] Conferences – See the following Conference Series: Finite elements in fluis I–IX, Wiley, Int. Conf. Num. Meth. Fluid Dyn. I–XII, Spinger Lecture Notes in Physics, AIAA CFD Conference I–XV, AIAA CP, Num. Meth. Laminar and Turbulent Flow, Pineridge Press, and others.
[6] E. Eaton, Aero-acoustics in an automotive HVAC module, American PAM User Conference, Birmingham, MI, October 24–25, 2001.
[7] M.D. Gunzburger, R. Nicolaides (Eds.), Incompressible Computational Fluid Dynamics: Trends and Advances, Cambridge University Press, Cambridge, 1993.
[8] Cooperative experiments on Wigley parabolic models in Japan, 17th ITTC Resistance Committee Report, 2nd ed., 1983.
[9] A. Jameson, W. Schmidt, E. Turkel, Numerical solution of the Euler equations by finite volume methods using Runge–Kutta time-stepping schemes, AIAA-81-1259, 1981.
[10] Y. Kallinderis, A. Chen, An incompressible 3-D Navier–Stokes method with adaptive hybrid grids, AIAA-96-0293, 1996.
[11] K.J. Karbon, S. Kumarasamy, Computational aeroacoustics in automotive design, computational fluid and solid mechanics, in: Proceeding of the First MIT Conference on Computational Fluid and Solid Mechanics, pp. 871–875, Boston, June, 2001.
[12] K.J. Karbon, R. Singh, Simulation and design of automobile sunroof buffeting noise control, 8th AIAA-CEAS Aero-Acoustics Conference, Breckenridge, June, 2002.
[13] J. Kim, P. Moin, Application of a fractional-step method to incompressible Navier–Stokes equations, J. Comput. Phys. 59 (1985) 308–323.
[14] Y. Li, T. Kamioka, T. Nouzawa, T. Nakamura, Y. Okada, N. Ichikawa, Verification of aerodynamic noise simulation by modifying automobile front-pillar shape, JSAE 20025351, JSAE Annual Conference, Tokyo, July, 2002.
[15] R. Löhner, A fast finite element solver for incompressible flows, AIAA-90-0398, 1990.
[16] R. Löhner, C. Yang, E. Onate, S. Idelssohn, An unstructured grid-based, parallel free surface solver, Appl. Numer. Math. 31 (1999) 271–293.
[17] D. Martin, R. Löhner, An implicit linelet-based solver for incompressible flows, AIAA-92-0668, 1992.
[18] R. Ramamurti, R. Löhner, A parallel implicit incompressible flow solver using unstructured meshes, Comput. Fluids 5 (1996) 119–132.
[19] H. Schlichting, Boundary Layer Theory, McGraw-Hill, New York, 1979.
[20] A. Takamura, M. Zhu, D. Vinteler, Numerical simulation of pass-by maneuver using ALE technique, JSAE Annual Conference (Spring), Tokyo, May, 2001.
[21] F. Thomasset, Implementation of Finite Element Methods for Navier–Stokes Equations, Springer, Berlin, 1981.
[22] P. Wesseling, Principles of Computational Fluid Dynamics, Springer, Berlin, 2001.